Inverse Analysis to Determine Hygrothermal Properties in Fiber Reinforced Composites

PAVANKIRAN VADDADI,* TOSHIO NAKAMURA AND RAMAN P. SINGH
Department of Mechanical Engineering, State University of New York at Stony Brook, NY 11794, USA

(Received August 26, 2005)
(Accepted December 9, 2005)

ABSTRACT: Fiber-reinforced composite laminates are often used in severe environments such as high temperature and humidity conditions. Therefore, it is of practical interest to establish a simple but robust method to determine material properties that define the hygrothermal behavior of composites under various conditions. In this article a novel inverse analysis approach is presented to identify the diffusivity, maximum moisture content, and coefficient of thermal expansion (CTE) and coefficient of moisture expansion (CME) of carbon fiber-reinforced epoxy matrix composites subjected to various conditions of environmental exposure. This procedure involves three distinct steps. First, the transient expansions and weight gains are experimentally measured under different temperatures and humidity conditions. Next, reference solutions are established from detailed computational models, which incorporate the heterogeneous nature of composite's microstructure. Finally, the Kalman filter technique is utilized to extract best estimates of the material parameters of interest. The use of inverse analysis is necessitated by the fact that backward relations from the measured parameters to the unknown properties are not directly apparent. The results show diffusivity to be a strong function of temperature while the maximum moisture content to be a strong function of relative humidity. For the case of material expansion, moisture induced strains as well as thermal strains exhibit slight dependence on temperature. In addition to estimating the material parameters of interest, detailed studies are conducted to investigate the source of scatterings observed in the expansion measurements during heating and moisture absorption, and possible 3D effects in measurements.

KEY WORDS: moisture diffusivity, moisture content, moisture expansion, thermal expansion, Kalman filter, fiber optic sensors.

*Author to whom correspondence should be addressed. E-mail: pvaddadi@ic.sunysb.edu
Figure 7 appears in color online: http://jcm.sagepub.com

0021-9983/07/03 0309–26 $10.00/0 DOI: 10.1177/0021998306063372

INTRODUCTION

CARBON FIBER-REINFORCED EPOXY matrix composites are used extensively in aerospace and other structural applications because of their high strength, high stiffness, and low density. However, harsh environmental conditions can cause deleterious effects on the mechanical properties and residual strength of these materials. Under high temperature and humidity, the composites undergo various thermophysical changes. Exposure to humidity causes moisture absorption and dilatational expansion in the polymer matrix. A large mismatch in the hygrothermal strains between the matrix and the fibers can generate large internal stresses which may affect gross performance of the composite [1]. Other studies [2–4] have also indicated that moisture absorption leads to changes in chemical characteristics of the epoxy matrix by plasticization and hydrolysis. Such effects are enhanced by concurrent exposure to ultraviolet (UV) radiation [5]. Hygrothermal exposure can lower both the elastic modulus and the glass transition temperature of polymer matrix [4,6–8]. Degradation can also lead to moisture wicking along the fiber–matrix interfaces, which reduces structural integrity. The major mechanical effects of environmental degradation are the deterioration of matrix-dominated properties such as compressive strength (lower critical loads for buckling and kink band formation), weakened interlaminar bonding in cross-plies, and lowered fatigue resistance and residual impact tolerance [2,6,7,9,10].

Several investigations have focused on the synergistic effects of moisture and temperature on the mechanical properties and durability of composites. Asp [11] studied the effects of these conditions on interlaminar delamination. The durability of graphite-epoxy composites under combined hygrothermal conditions was also investigated [12] and the accumulation and progression of fatigue damage was found to depend on the environment. Choi et al. [8] reported on the effects of fiber volume fraction, void fraction, and ply orientations on the moisture absorption rate of carbon-epoxy fiber composites. They noted that the moisture absorption behavior is affected by the temperature history, and that the diffusivity increases with matrix volume fraction and void fraction. These studies illustrate the importance of hygrothermal behavior in determining the durability and residual strength of composites subjected to environmental exposure. The moisture diffusion process can be characterized by the diffusivity and the maximum moisture content while the deformation due to moisture absorption or temperature is characterized by coefficient of moisture (CME) and coefficient of thermal expansion (CTE), respectively.

The objective of the current work is to evaluate a novel inverse analysis approach to determine the hygrothermal parameters of fiber-reinforced composites. These parameters are normally functions of the environmental exposure conditions (i.e., temperature and relative humidity). Loos and Springer [13] found that the maximum moisture content is a strong function of the relative humidity of the exposure environment while the diffusivity is a strong function of the temperature. In general, the maximum moisture content is determined by exposing the material to a given relative humidity for a sufficiently long time until the limiting saturation is attained and the specimen does not absorb moisture any further. Obviously, this process is time consuming and often cumbersome. In the proposed procedure, the test duration can be shortened significantly by extrapolating the maximum moisture content from the record of transient moisture absorption measurements.

In general, effective or averaged properties are used to characterize the overall behavior of composites. Such properties may be obtained either with a rule-of-mixtures approach or by numerical analyses. While the use of effective properties is appropriate for steady-state conditions, their applicability for transient conditions is, at best, questionable. More specifically, under transient conditions, the effective properties do not describe the time and spatial variations of the parameters of interest accurately (e.g., local moisture content).

Previously, we have estimated the diffusivity and the maximum moisture content using experimental measurements of relative weight gain for composite specimens exposed to hygrothermal conditions [14]. In the present investigation, to estimate additional parameters (i.e., the CTE and CME), weight as well as expansion were measured. Furthermore, an appropriate inverse analysis algorithm was established to accommodate the multiple measurements as well as the increased number of unknowns. In the tests, expansions due to moisture absorption and temperature variation were recorded using fiber-optic strain sensors. These sensors offer numerous advantages over conventional resistive foil strain gages through increased resolution and accuracy, insensitivity to electromagnetic interference and the capability of use at high temperature and moisture conditions. In recent years, fiber-optic sensors have been increasingly used for strain measurements in composites due to their small size and ability to be embedded or bonded inside the material [15–17]. In the present experiments, the primary advantage of fiber-optic strain sensors, over more conventional stain gages, is not only their insensitivity to the electromagnetic noise inside the environmental chamber but also their long-term durability in harsh environments.

Since the response times of moisture transport and thermal expansion are very different, two separate tests were conducted to quantify the parameters. First, in order to measure the moisture absorption behavior, specimens were placed in an environmental chamber for up to 1200 h (50 days) under various humidity and temperature conditions. To measure the CTE, specimens were kept in the chamber for much shorter durations (i.e., minutes). Since the thermal equilibrium is reached several orders of magnitude faster than the moisture saturation, the transient thermal parameters (e.g., thermal conductivity) of composites were not determined here. On the other hand, the transient characteristics of moisture flow are very important, and thus the diffusivity, CME, and the maximum moisture content were estimated under various temperatures and humidity conditions, as they were considered to be functions of temperature and humidity. The integrated experimental and inverse analysis approach employed in this investigation is described next.

EXPERIMENTAL PROCEDURE

Composite Specimen

Specimens were machined from commercially fabricated laminates of IM7/997 carbon-fiber reinforced epoxy donated by Cytec Engineered Materials, Inc. (Anaheim, California). This composite is under development for application to aerospace and expected to provide higher damage tolerance than currently qualified materials such as IM7/5271-1 [18]. These laminates consist of PAN based, 5 μm diameter IM7 carbon

Table 1. Mechanical properties of IM7 carbon fiber and 997 epoxy.

Property	IM7 fiber	997 epoxy
Young's modulus (GPa)	20 (transverse)	4.14
Poisson's ratio	0.33	0.36
Tensile strength (MPa)	5150	90
Density (kg/m^3)	1780	1310

fibers (Hexcel Composites, Inc., Connecticut) in a 997 matrix, which is a 177°C (350°F) curing, thermoplastic modified, toughened epoxy resin using a proprietary formulation. This epoxy is often used in applications where impact resistance and excellent hot/wet performance is critical. The average fiber volume fraction for these laminates was determined to be $58 \pm 1\%$ based on microtomography conducted on polished cross-sections. The known properties of the IM7 fibers and 997 epoxy are listed in Table 1.

For the tests, several specimens were prepared from 8-ply unidirectional laminates (i.e., $[0]_8$), with dimensions of $140 \times 70 \times 1.2$ mm. Although only unidirectional laminates were considered here because of the simplicity of experimental interpretation, the properties of the epoxy phase (not the entire composite) should be essentially identical for cross-ply and other laminates as well. The specimens were machined using a water-cooled, high-speed diamond saw, following which, the edges were polished using 120, 400, and 600 grit metallographic paper to remove any microstructural damage. The high temperature and moisture absorption tests were conducted with an environmental chamber (Benchmaster BTRS, Tenney Environmental, Williamsport, Pennsylvania). This chamber provides automated exposure to various conditions of temperature and humidity for extended durations of time. The thermal expansion tests were conducted in a bench-top muffle furnace (LMF A550, Omega Engineering Inc., Stamford, Connecticut).

Fiber-optic Strain Sensors

Extrinsic Fabry-Perot-based fiber-optic sensors (FISO Technologies, Quebec, Canada) were used to measure transient strains in composites exposed to various temperature and humidity conditions. These sensors are well suited for measurements in harsh environments because of their small size, resistance to corrosive environments, immunity to electromagnetic interference, and high temperature range. Signals from fiber-optic sensors were supplied to a DMI (desktop management interface) multichannel signal conditioner to record the strains. The DMI signal conditioner is controlled through a PC using the FISO-Commander software. The schematic of measurement arrangement is shown in Figure 1(a).

The sensing element of the fiber-optic transducer is of an interferometric type. The sensing element is designed such that a stimulus, which is the physical parameter being measured, produces a change in the cavity length of the Fabry-Perot interferometer. This change can be observed from the output signal of the fiber-optic transducer, which then can be related to strain measurement. In EFPI sensor, an external light source is coupled to the lead-in fiber, which is bonded inside a small portion of a hollow core fiber. A portion of light reaching the sensor is reflected at the face of the lead-in fiber end,

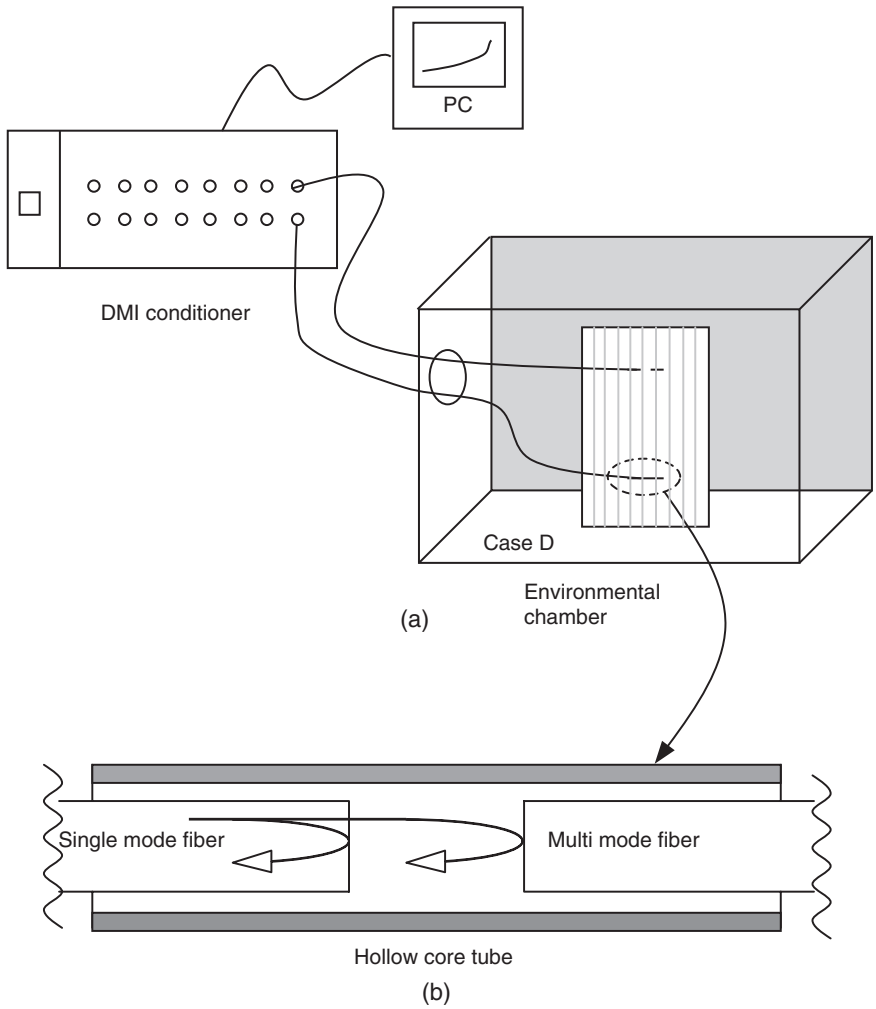

Figure 1. *(a) Schematic of data acquisition system to measure strain of specimen in environmental chamber. (b) Illustration of the fiber optic sensor.*

while the rest travels through the air gap and is partially reflected at the fiber end. The light reflected back from the two surfaces is transmitted back to the lead-in fiber and deformation can be measured from the change in gap length. The free end of the sensor is connected to the DMI conditioner, as shown in a schematic of the sensor operation in Figure 1(b). The conditioner samples the transducer signal at a fixed rate of 20 Hz, and the readings are averaged for a given period of time and stored as measured records. For each specimen, two sensors (one on each surface) were bonded transversely with respect to the carbon fiber direction as illustrated in Figure 1(a). Here, only the transverse or normal strain perpendicular to the fiber direction was measured because of its greater expansion. An accessory hole in the environmental chamber allowed for strain measurements to be conducted during the environmental exposure. Although the current test placed the sensors on the free surfaces, fiber-optic sensors can be also embedded within the composites during their fabrication process. Then the proposed inverse analysis

can readily accommodate such internal strain measurements to estimate the unknown properties.

Bonding of the fiber-optic sensors required special care due to their small size and high sensitivity. First, the specimen surface was cleaned with acetone followed by dry and wet abrasion with sand paper. The fiber-optic gage was then held onto the specimen with an electric tape in the desired orientation and a 5-min epoxy was used 3 mm from the gage-sensitive region to ensure proper alignment with specimen. Subsequently, the adhesive was applied, taped, and allowed to cure. To adhere the fiber-optic sensor to the surface, it was shielded with a thin epoxy layer ($\sim$100 μm thick). These steps follow the procedure recommended by FISO technologies. Although, the thickness of the extra layer is small, it may still act as a barrier to moisture absorption and consequently alter expansion characteristics of composites. In order to quantify its effect, a detailed computational analysis was carried out and described in the Appendix. The analysis essentially confirms such an effect to be minimal and that it does not influence the estimations of unknown parameters.

Weight Measurements

Another measurement parameter was the weight gain of composites due to moisture absorption under various environmental conditions. For each exposure condition, the weight gain was monitored for two nominally identical specimens placed in the environmental chamber. These specimens were additional to those used for monitoring strains with fiber-optic sensors. The separate specimens were necessary due to difficulty in measuring the weights of specimens with fiber-optic sensor attached. During the tests, two specimens were taken out of the chamber every 24 h. The surfaces were dried carefully and the weights were measured using an analytical balance with a resolution of 0.1 mg, which corresponds to $\sim 5 \times 10^{-4}\%$ of the specimen weight. After they were weighed, the specimens were immediately placed back in the chamber. The entire process required $\sim$5 min. It should also be noted that all specimens were preconditioned at 50°C for 2 weeks until no change in weight was observed. This process ensures that the specimens are uniformly dry prior to environmental exposure.

Moisture Absorption Tests

In order to determine the individual effects of relative humidity (R_H) and temperature (T), four separate environmental conditions were considered:

$$\begin{aligned}
&\text{Case A}: T = 85^\circ\text{C} \quad \text{and} \quad R_H = 85\%,\\
&\text{Case B}: T = 40^\circ\text{C} \quad \text{and} \quad R_H = 85\%,\\
&\text{Case C}: T = 85^\circ\text{C} \quad \text{and} \quad R_H = 50\%, \quad \text{and}\\
&\text{Case D}: T = 40^\circ\text{C} \quad \text{and} \quad R_H = 50\%.
\end{aligned}$$

These conditions encompass a range of hygrothermal environments of interest. In the analysis, it was assumed that moisture absorption occurs only in the epoxy matrix and not in the carbon fibers. For each environmental condition, the chamber was allowed

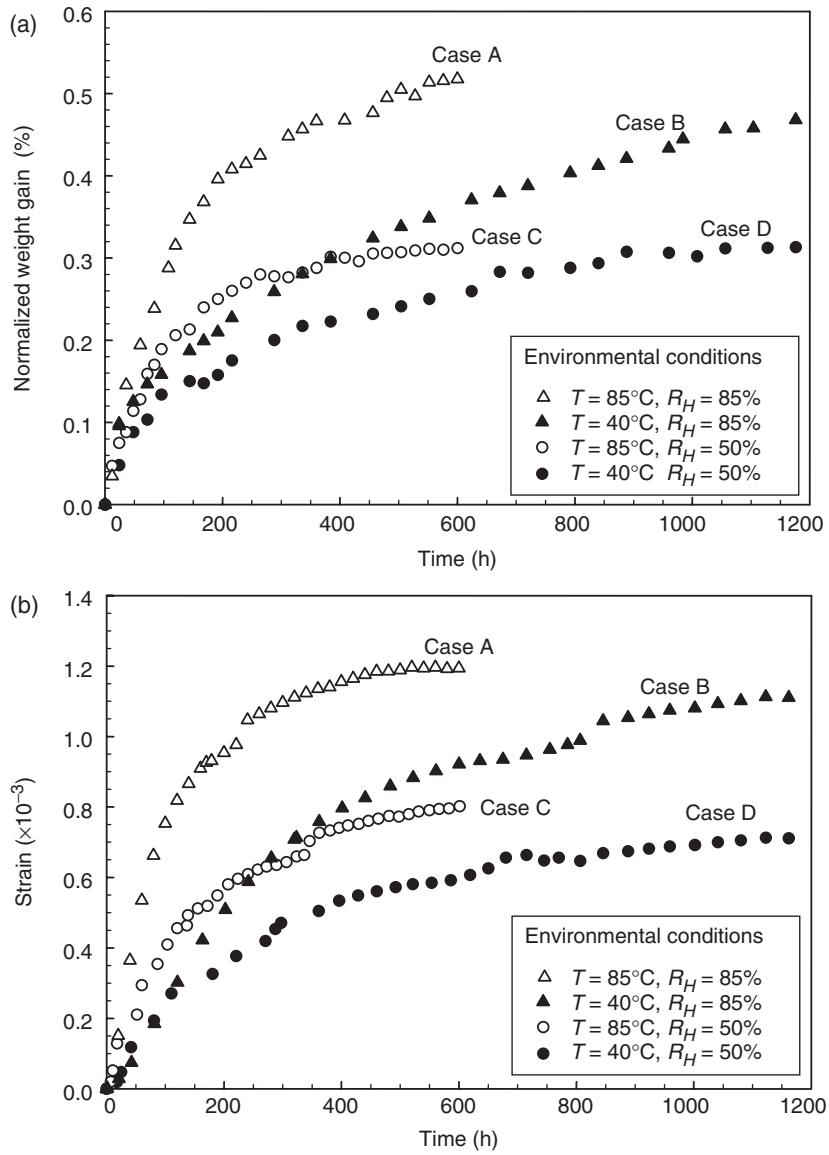

Figure 2. *Experimental measurements of: (a) weight gains due to moisture absorption and (b) transverse strains due to moisture expansion, shown as functions of time under different environmental conditions.*

to stabilize and the strain sensors were initialized to eliminate any effects of expansion due to the temperature.

The normalized weight gain and transverse strain (perpendicular to fibers) measurements for the four environmental conditions are shown in Figure 2. The normalized weight change is obtained by dividing the increase in weight by the initial dry weight of specimen. For the lower temperature tests (Cases B and D), the specimens were kept in the chamber for 1200 h (50 days) while for the high temperature tests, (Cases A and C), the specimens were kept in the chamber for about 600 h (25 days). For each condition,

the plots show average values obtained from two separate specimens. Typical differences in the normalized weight changes of two specimens were ~1%. Similarly, the fiber-optic strain measurements on the top and bottom surfaces of any given specimen differed by less than 1%.

For Case A ($T = 85°C$ and $R_H = 85\%$), a rapid increase in both weight gain and strain was observed during the initial periods of exposure, followed by slower changes. This was expected as the kinetics of diffusion is driven by the absorbed moisture gradient, which is high during the initial phases and reduces as the specimen saturates. When the temperature was lowered to $T = 40°C$ while keeping the R_H fixed at 85% (Case B), a longer time was needed to achieve the saturation. Nevertheless, for both Cases A and B, the specimens appeared to approach similar limiting values (full saturation), respectively. In contrast, when the R_H was lowered to 50% while maintaining the temperature at $T = 85°C$ (Case C), the composite required similar time to reach the saturation but at a lower level as compared to Case A. When both T and R_H were lowered to $T = 40°C$ and $R_H = 50\%$, respectively (Case D), again a longer time was needed to saturate for both weight gain and strain.

In Figure 2, one can also observe that the measurement curves are not smooth. For weight change, these variations may be explained by the manual wiping of specimens prior to the weighing that can introduce small error. On the other hand, smoother variations were expected for the strain measurements since the specimens were untouched and kept in the chamber throughout the tests. The cause of discontinuous strain change is closely analyzed in conjunction with the thermal cycle tests presented in the 'Thermal Expansion' section.

Thermal Expansion Tests

The thermal expansion of composite specimens was measured over a 20–120°C temperature range. Composite specimens were exposed to various temperatures and the surface strains were monitored using fiber-optic sensors. Two gages were bonded on the two surfaces of the composite specimen in order to ensure the measurement accuracy. To check for consistency, metal strain gages were also bonded onto the specimen. In addition, a separate aluminum plate with strain gages was placed in the same environmental chamber to further monitor the testing environments.

Initially, the specimens were placed in the chamber at 20°C and the temperature was incrementally raised up to 120°C in about 20 min. At each temperature, the system was allowed to stabilize for about a minute. The temperature was measured by an independent thermocouple in the chamber. In order to ensure the accuracy of the strain measurements, at the end of the test, the temperature was again lowered to room temperature and subsequently raised directly to intermediate values, allowed to stablize and the strains were compared with the earlier measurements.

The measured thermal strains of composites are shown as a function of temperature in Figure 3. Note that the thermal strain of aluminum plate essentially increased linearly with the temperature, assuring the accuracy of the testing condition. As observed in the figure, the strain changes of composite were highly uneven during the first heating (note: these are from virgin specimens). At first, the cause was thought to be the inhomogeneous nature of composite microstructure. However as the thermal tests were repeated, a lesser scattering was observed in the measurements. In fact, at the ninth heating cycle, the strain

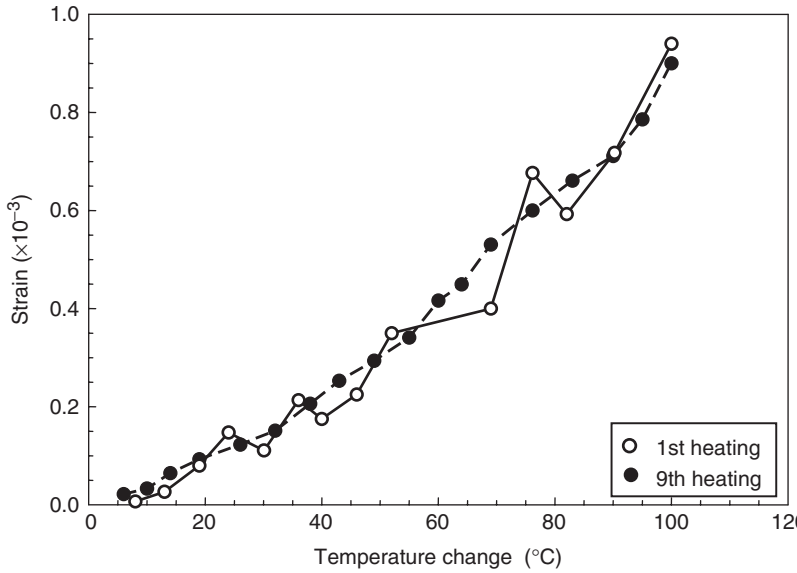

Figure 3. *Measured transverse strains due to thermal expansion, shown as functions of temperature change during 1st and 9th heating cycles.*

increase became smooth as shown in the figure. A separate specimen was tested to confirm this behavior. Based on additional analysis (discussed in the 'Thermal Expansion' section), we postulate the cause of initial irregular strain change to be residual stresses distributed unevenly within the composite. As the specimens are thermally cycled, these trapped stresses are relaxed and the oscillatory behavior disappears.

INVERSE ANALYSIS

A procedure based on inverse analysis is introduced to extract the unknown parameters of interest from the experimental measurements. When the explicit relations from measured records to unknown state parameters are not obvious, inverse analysis techniques provide an effective approach to extract estimates. Here, the inverse procedure is formulated to estimate the three unknown parameters from two measurements.

In this analysis, instead of treating the composite as a homogenized material and determining its effective properties, the unknown state parameters were defined as the properties of epoxy matrix. This approach has several advantages. First, when an analysis requires discrete microstructural modeling (e.g., to determine internal state such as residual stresses), the properties of individual constituents must be known. Second, for the moisture diffusion, where transient behavior is critical, a homogenized model cannot describe the time-varying absorption process accurately. The error caused by homogenized model during transient moisture absorption was quantitatively determined by Vaddadi et al. [14]. Once properties of individual constituents are known, the effective properties of composite can be easily obtained via analytical (e.g., rule-of-mixture) or computational models.

It should be also noted that one may opt to seek these parameters from bulk epoxy. However, in many instances, same particular epoxy is not available in bulk form, and also the curing process during composite fabrication may not produce identical properties. In addition, the present procedure also allows for the testing of aged composites to determine their modified moisture transport characteristics. Another advantage of directly determining epoxy properties of already fabricated composite is that it considers other effects such as small voids/cracks introduced during processing, and possible decohesion at fiber–matrix interfaces. These process-induced effects are implicitly included in the estimated properties of epoxy, and thus are more suitable in modeling of matrix–fiber composites.

In the current study, the unknown parameters are the maximum moisture content, C^*, the diffusivity, D, the coefficient of moisture expansion (CME), β, and the CTE, α of the epoxy matrix. The last parameter is determined independently from the thermal test. Since the carbon fibers absorb very little moisture, their diffusivity, maximum moisture content, and coefficient of moisture expansion were assumed to be zero. The CTE of carbon fibers was treated as known since its value is well documented. For the inverse analysis technique we employ the Kalman filter, which has been widely used in many areas of engineering, such as sensor calibration, tracking applications, trajectory determination, and image and signal processing [19–22]. It has been also used for the estimation of various unknown material parameters [23–25]. The main advantage of the Kalman filter algorithm over other adaptive algorithms is that it is highly effective in nonlinear systems and has a fast convergence to optimal solutions. In addition, due to its mathematical structure, it has the ability to filter out measurement noise and error. These properties make the technique ideally suited for the present investigation since the moisture absorption process is nonlinear with time, and the measurements can contain some errors. Prior to implementing this technique, it must be carefully tailored and adopted to the present analysis, as described next.

Kalman Filter Procedure

In the Kalman filter formulation, the three unknown parameters are denoted in a vector form as $\boldsymbol{X}_t = (C_t^*, D_t, \beta_t)^T$, where C_t^*, D_t, and β_t are the current estimates of the maximum moisture content, diffusivity, and coefficient of moisture expansion of epoxy, respectively. Here t may represent the actual time as well as a pseudotime such as a step/increment number that ranges $0 \le t \le t_{\max}$. The successive estimates are indirectly made from the measured weight gain, w_t^{meas}, and moisture induced strain, $\varepsilon_t^{\text{meas}}$, which may contain error/noise as $w_t^{\text{meas}} = w_t + w_t^{\text{err}}$, and $\varepsilon_t^{\text{meas}} = \varepsilon_t + \varepsilon_t^{\text{err}}$, respectively. At $t = 0$, the initial estimates C_{o}^*, D_{o}, and β_{o} are assigned and the subsequent estimates are made according to the following algorithm.

$$\boldsymbol{X}_t = \boldsymbol{X}_{t-1} + \boldsymbol{K}_t\left[\boldsymbol{M}_t^{\text{meas}} - \boldsymbol{M}_t(\boldsymbol{X}_{t-1})\right]. \tag{1}$$

Here, $\boldsymbol{K}_t$ is the 'Kalman gain matrix' and $\boldsymbol{M}_t^{\text{meas}}$ is a vector containing measured record of weight gain w_t^{meas} and the strain $\varepsilon_t^{\text{meas}}$ (i.e., $\boldsymbol{M}_t^{\text{meas}} = w_t^{\text{meas}}, \varepsilon_t^{\text{meas}})^T$) at t. Also $\boldsymbol{M}_t(\boldsymbol{X}_{t-1})$ is a vector containing measured parameters computed with estimated unknown state parameters at the previous step. Note that these computations require solutions of

measured parameters for a given set of state parameters. Such solutions are sometimes referred as the 'forward' solutions. In the above equation, the Kalman gain matrix multiplies the difference between the measured and computed values of the weight gain and strain to make corrections to the unknown state parameters. The Kalman gain matrix is computed as

$$\boldsymbol{K}_t = \boldsymbol{P}_t \boldsymbol{M}_t'^T \boldsymbol{R}_t^{-1} \quad \text{where} \quad \boldsymbol{P}_t = \boldsymbol{P}_{t-1} - \boldsymbol{P}_{t-1}\boldsymbol{M}_t'^T\left(\boldsymbol{M}_t'\boldsymbol{P}_{t-1}\boldsymbol{M}_t'^T + \boldsymbol{R}_t\right)^{-1}\boldsymbol{M}_t'\boldsymbol{P}_{t-1}. \tag{2}$$

With three state and two measured parameters, the dimensions of Kalman gain matrix are 3×2. Also $\boldsymbol{M}_t'$ is a 2×3 matrix that contains the gradients of $\boldsymbol{M}_t$ with respect to the state parameters C^*, D, and β as

$$\boldsymbol{M}_t'^T = \frac{\partial \boldsymbol{M}_t}{\partial \boldsymbol{X}} = \begin{pmatrix} \dfrac{\partial w_t}{\partial C^*} & \dfrac{\partial w_t}{\partial D} & \dfrac{\partial w_t}{\partial \beta} \\ \dfrac{\partial \varepsilon_t}{\partial C^*} & \dfrac{\partial \varepsilon_t}{\partial D} & \dfrac{\partial \varepsilon_t}{\partial \beta} \end{pmatrix}. \tag{3}$$

In addition, $\boldsymbol{P}_t$ is the 'measurement covariance matrix' related to the range of unknown state parameters at increment t, and, $\boldsymbol{R}_t$ is the 'error covariance matrix', related to the size of measurement error. Once the initial values are imposed, $\boldsymbol{P}_t$ is updated every step, while $\boldsymbol{R}_t$ is prescribed at each step. However, in many cases, fixed values can be assigned to the components of $\boldsymbol{R}_t$ as long as measurement error bounds do not vary substantially during the duration of measurements. Since the convergence rate is sensitive to the values of $\boldsymbol{P}_t$ and $\boldsymbol{R}_t$, proper assignments for these two matrices are essential. After several trials, the initial measurement covariance matrix and the constant error covariance matrix were assigned in this analysis as

$$\boldsymbol{P}_o = \begin{bmatrix} (\Delta C^*)^2 & 0 & 0 \\ 0 & (\Delta D^*)^2 & 0 \\ 0 & 0 & (\Delta\beta)^2 \end{bmatrix} \quad \text{and} \quad \boldsymbol{R}_t = \begin{bmatrix} 10R_w & 0 \\ 0 & 10R_\varepsilon \end{bmatrix}. \tag{4}$$

Here ΔC^*, ΔD, and $\Delta\beta$ denote the expected ranges of the unknown parameters, respectively. While $\boldsymbol{P}_o$ is diagonal, the procedure results in a filled $\boldsymbol{P}_t$ matrix during subsequent increments. In the current analysis, the diagonal components of $\boldsymbol{R}_t$ are chosen based on the estimated measurement error for the weight and the strain measurements. Here $10R_w$ and $10R_s$ denote 10 times the normalized estimated maximum errors of the weight and strain measurements. Based on the experimental measurements, as shown in Figure 2, dimensionless R_w and R_s were estimated as 2×10^{-3} and 8×10^{-3}, respectively. In general, larger values lead to slower but stable convergence to the solutions of unknown state parameters. The Kalman filter procedure, which is summarized in Figure 4, was implemented in a computational code.

As noted earlier, the Kalman filter requires the solutions of weight gain w_t, strain ε_t, and their gradients $\boldsymbol{w}_t'$ and ε_t' for given values of C^*, D, and β at a given time (i.e., forward solutions). For some problems, these solutions may be obtained from closed-form analytical solutions or simple numerical calculations. However, in many cases involving complex boundary and geometrical conditions, the solutions can be obtained only through separate analyses. For moisture diffusion problems, they can be approximated using the

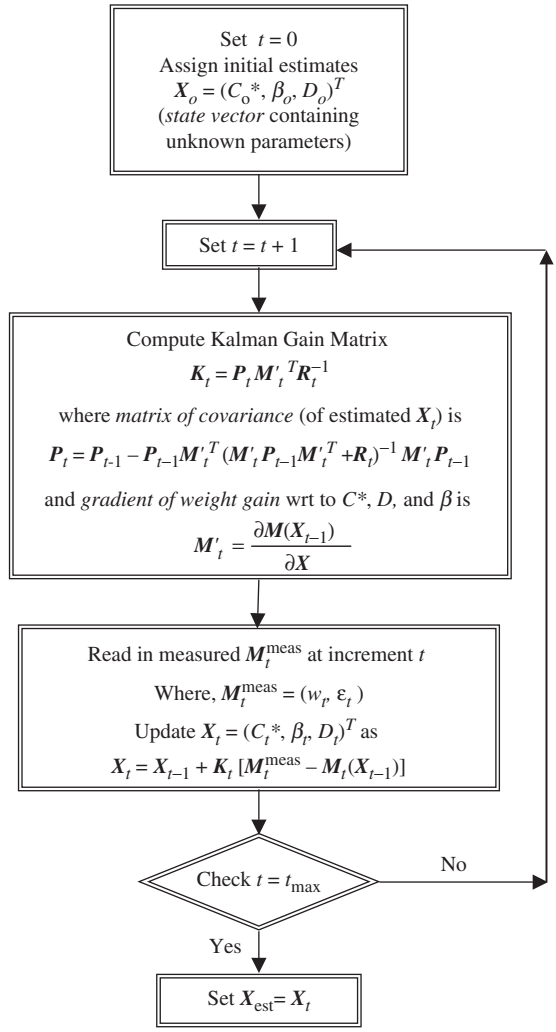

Figure 4. *Flowchart for Kalman filter to estimate maximum moisture content, diffusivity, and coefficient of moisture expansion from time history measurements of strain and weight gain.*

Fickian equation in a homogenized model without resorting to detailed computations. Such a procedure, however, was found to be inaccurate for transient moisture transport in composites, as previously discussed. Thus, detailed finite element simulations were carried out for the moisture absorption process to generate accurate functions for w_t, ε_t, $\boldsymbol{w}'_t$, and ε'_t, as discussed in 'Finite Element Simulations'.

Reference Data and Domain of Unknowns

The Kalman filter algorithm requires time-varying solutions of weight gain and strain as functions of the unknown state parameters. As no simple solutions are available, which explicitly account for the heterogeneous constitution of composites, finite element

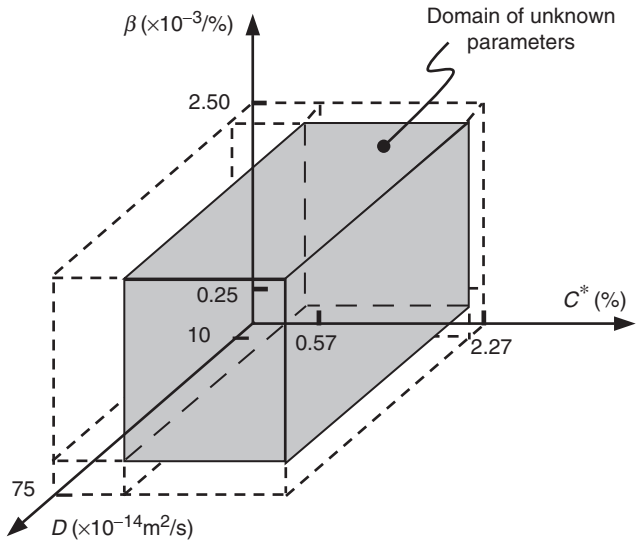

Figure 5. *Domain of unknown state parameters shown in 3D space defined by maximum moisture content C*, diffusivity D, and moisture expansion coefficient β. Best estimates are explored within the domain.*

simulations were carried out to establish the reference data or forward solutions. The reference data comprise of time-dependent variations of strain, weight gain, and their gradients for various values of C^*, D, and β.

Prior to determining the reference solutions, it is necessary to set bounds or a domain for the unknown parameters. The required domain can be approximated either from available information regarding the unknown state parameters or from comparison of the experimental measurements and results of a few trial simulations. Here, both approaches were used to select the domain for the maximum moisture content C^*, diffusivity D, and coefficient of moisture expansion β. A schematic of three dimensional (3D) domain is shown in Figure 5, where the values were set as $0.57\% \leq C^* \leq 2.27\%$, $10 \times 10^{-14}\text{m}^2/\text{s} \leq D \leq 75 \times 10^{-14}\text{m}^2/\text{s}$, and $0.25 \times 10^{-3}/\% \leq \beta \leq 2.5 \times 10^{-3}/\%$, respectively. The unit of C^* is weight percent of water (H_2O), and the unit of β is per weight percent of H_2O. Since computations with many different sets of state parameters would be prohibitive, we utilized cubic Lagrangian interpolation functions. Here sixty-four ($=4 \times 4 \times 4$) base points were chosen and the finite element simulations were performed for specified sets of C^*, D, and β. At each set of state parameters, solutions of weight and strain were stored for every 24-h time increment. When w_t and ε_t at any intermediate values of C^*, D, and β were required, they and their gradients were interpolated with the cubic Lagrangian functions. This approach was found to be very accurate as long as the measured parameters were sufficiently smooth functions of the state parameters.

Finite Element Simulations

In the finite element analysis, we capture the heterogeneous microstructure using randomly distributed fibers to model the fiber-reinforced composite. The motivation to

adopt such a model was threefold. First, a homogenized model does not simulate accurate transient behavior of moisture diffusion as described previously. Detailed comparison study with 1D Fickian model is shown in [14]. Second, unit cell models, popular in many composite analyses, cannot be used here since the moisture transport occurs across the entire thickness. Third, again due to the transient nature of the problem, models with regularly spaced fibers (e.g., hexagonal packing) do not offer sufficiently accurate solutions. Thus, the random nature of fiber distributions is essential in capturing characteristics of transient moisture transport in the fiber-reinforced composites (as discussed in detail in [14]). These conditions led us adopt the random fiber model that has good resemblance to the microstructure of actual specimens.

The specimen has eight plies totaling a thickness of 1.2 mm. Figure 6(a) shows the geometric model of the composite specimen and the considered section. Due to the symmetry across the center-plane, only one-half thickness of the composite is modeled. The effects of edges can be effectively ignored since the total area of the front/back surfaces is much greater than the edge area (by a factor of 37). This reduces the problem to be two-dimensional (2D). In the analysis, both the moisture absorption as well as the expansion due to the moisture was considered. The fibers were placed randomly within the domain with a computational code. Special algorithms were required to position fibers beyond a volume fraction of 50% since the space available to place extra fibers diminishes greatly. The program rearranges the initially placed fibers to optimize the available space and then restarts to place fibers in the modified configuration. This process is repeated until the desired volume fraction is achieved. The model width is set to 64 μm, which has about 10 fibers distributed across. The final model contains about 1200 fibers, totaling the given fiber volume fraction of 58%.

Once the random fiber geometric model was created, a mesh generator code was utilized to construct the finite element mesh shown in Figure 6(b) and (c). The element sizes were kept sufficiently small for accurate simulation of transient moisture transport and deformation analysis. The entire mesh contains more than 130,000 nodes and 240,000 triangular generalized plane strain elements. Although detailed convergence analysis was not possible due to mesh complexity, two additional meshes with different random fiber distributions were constructed to check for the consistency. The solutions from the three models showed essentially identical results.

The transient moisture induced deformation was studied in a coupled temperature–displacement analysis of the finite element analysis [26]. The analogy between Fick's law for mass diffusion and Fourier's law for heat transfer was employed to model transient moisture diffusion [27]. The values of conductivity, specific heat, and density, for a heat transfer analysis, were adjusted appropriately to provide solutions for transient moisture diffusion. For the boundary conditions, symmetry conditions in moisture, displacement, and temperature were imposed along the sides of the model except along the exposed surface. For the symmetry conditions, the three sides were kept straight and the four corners were set to remain perpendicular to represent an infinitely wide laminate For the finite element model, moisture flows only across the top surface exposed to the humidity. Thus, it was possible to specify the maximum moisture content for given environmental conditions as the boundary condition on this surface. At time $t = 0$, the entire specimen had zero moisture content. For $t > 0$, a fixed level of moisture condition is imposed along the top for each condition. The computational analysis of moisture diffusion was carried out over the respective duration of experimental tests (either 600 or 1200 h). As the moisture is transported and absorbed through the specimen, the total weight increases and the

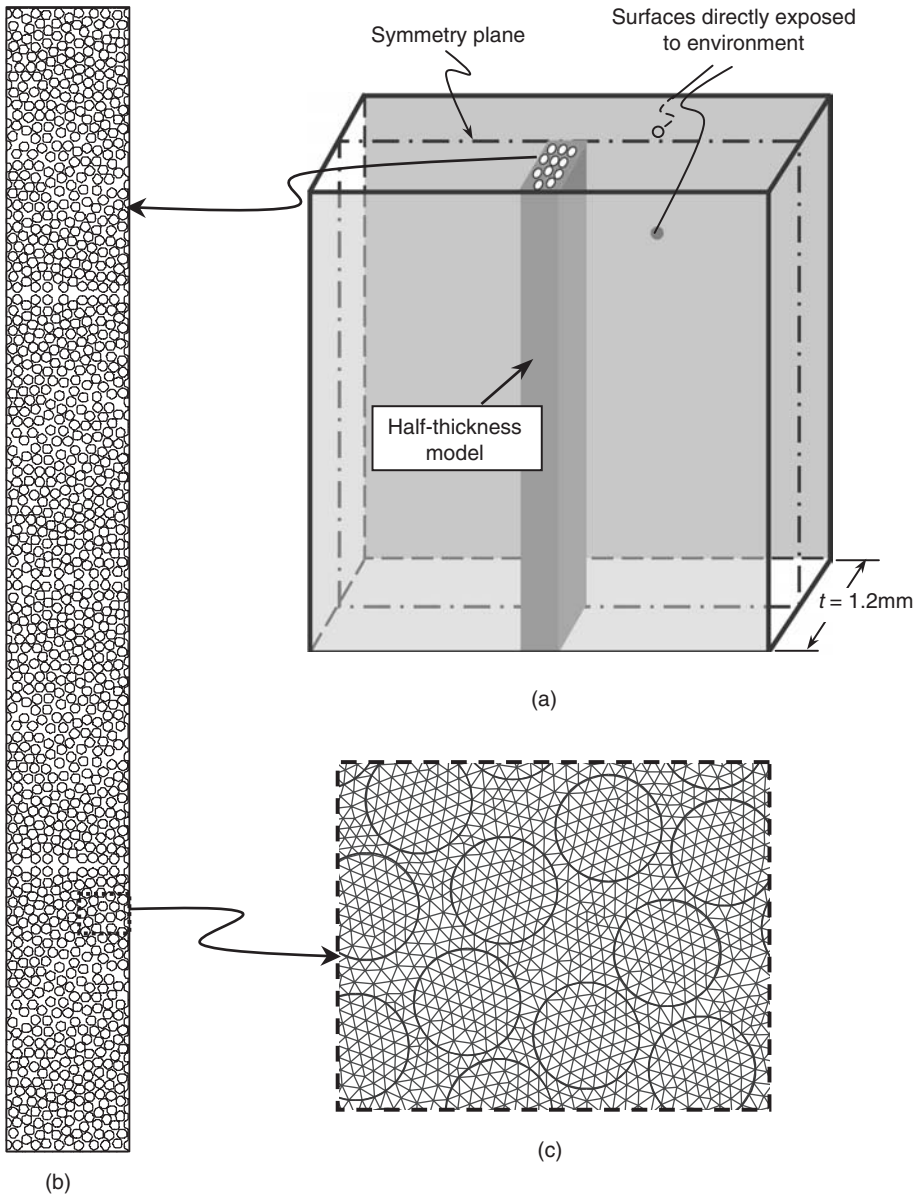

Figure 6. *Schematics of random fiber model used in the finite element transient analysis: (a) physical model; (b) outlines of 1200 fibers in the half-thickness model; and (c) enlarged view of mesh with fibers.*

epoxy phase undergoes dilatational expansion. The total weight gained by the specimen was obtained by numerically integrating moisture content of all elements every 24 h.

Moisture absorption and temperature change result in stresses associated with hygrothermal expansion in the composites. The linear constitutive relationship for the epoxy can be shown as

$$\sigma_{ij} = \lambda \varepsilon_{kk} \delta_{ij} + 2\mu \varepsilon_{ij} - (3\lambda + 2\mu)(\beta \Delta C + \alpha \Delta T)\delta_{ij}, \tag{5}$$

where λ and μ are the Lame constants. Although not shown, our computational results estimated that the internal stresses to reach as high as 50 MPa in tension at certain locations where multiple fibers are clustered. These high stresses can initiate matrix cracking and debonding of the matrix and fibers.

ESTIMATION OF HYGROTHERMAL PROPERTIES

Transient Moisture Absorption

The best estimates of moisture-related material parameters were extracted using the Kalman filter with available measurements and reference data. The Kalman filter is based on an incremental approach and updates the estimates with the measured weight and strain that were provided at every time increment. At the first increment, initial estimates of unknown parameters must be assigned. In general, the final converged estimates are not identical for different initial estimates. In our unique procedure to identify the best estimates, the Kalman filter was carried out with many different initial estimates of C^*, D, and β with their values spread evenly (at $40 \times 40 \times 40$ points) in their domain of unknowns (Figure 5). For each set of initial estimates, the Kalman filter computed the final estimates. In order to illustrate different locations of final estimates, contour plots were constructed. These intensity of convergence plots can then be used to identify most likely values of best estimates. A location with high contour value signifies that more initial estimates converged near the particular values of C^*, D, and β. Thus best estimates can be taken at the highest intensity of convergence.

The results of Kalman filter for different environmental conditions are shown in Figure 7. Here, the contour values are normalized so that the highest intensity takes the value of 100. Although three unknowns were estimated simultaneously, their intensity of convergence is shown in two separate 2D plots for clarity. Here, in each plot, convergence intensity of two out of the three parameters is shown. Although another plot with the remaining combination is available, it is not shown to save space. Figure 7(a) shows the results of Case A with $T = 85^\circ$C and $R_H = 85\%$. For this case, the best estimates of the unknown state parameters were identified as $C^* = 1.45\%$, $D = 54.3 \times 10^{-14}\,\mathrm{m^2/s}$, and $\beta = 1.89 \times 10^{-3}/\%$, respectively. Note the highest intensity was determined from all three parameters and it may not necessarily coincide with that of the two parameter plots shown in the figures. Similar convergence results were obtained for the other three cases as shown in Figure 7(b), (c), and (d), respectively. The summary of best estimates for various environmental conditions is presented in Table 2. These results clearly exhibit their dependence on the relative humidity and/or temperature. The most significant influence is observed in the temperature dependence of diffusivity.

As noted earlier, the strength of inverse analysis approach lies in its ability to estimate unknowns with limited data. In order to illustrate this point, separate analyses were performed with shorter time durations of experimental measurements. For example, for Case A ($T = 85^\circ$C and $R_H = 85\%$), only first 360 h of weight and strain measurements were used instead of measurements over 600 h. The results of best estimates obtained with reduced experimental records are shown in Table 3. Although differences in the estimates can be observed in each case, they are generally within 5% of the estimates made with the full measurements shown in Table 2. For Cases B and D, the reduction in time period is 480 h (20 days), which represents significant savings in the long-term tests. These results

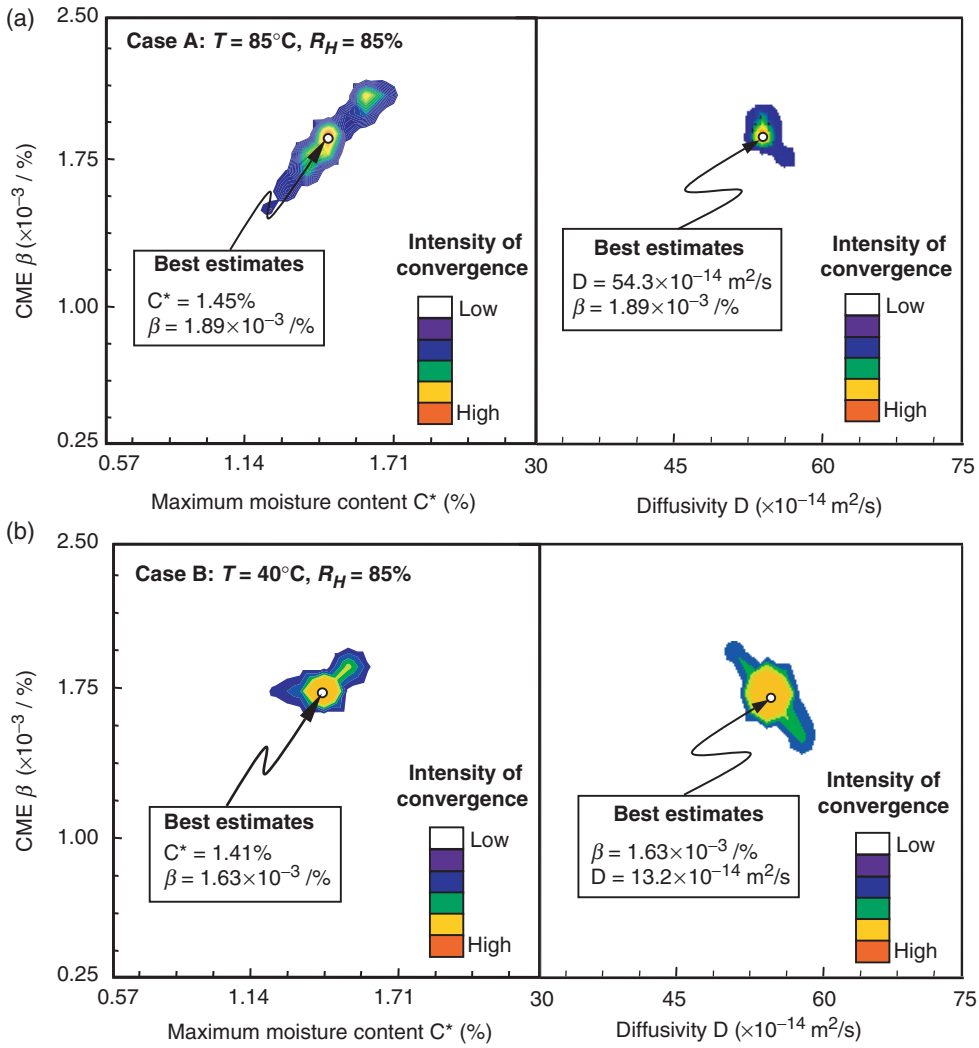

Figure 7. *Results of Kalman filter for different environmental conditions.*

demonstrate that the present method is effective in estimates unknowns with data only from transient stage. This feature is particularly attractive for lower temperature tests when complete saturation can take much longer times.

In most inverse problems, there is no independent way to prove the best estimates are indeed close to the correct solutions. However, there are two ways to assess the likeliness of accuracy. One is from the sizes of converged regions shown in the intensity of convergence plots. A small region implies that the inverse method is robust since many initial estimates converged near the same location (i.e., similar estimates). The converged regions shown in Figure 7 are reasonably contained, which suggests reasonable accuracy of best estimates. An additional confirmation can be made from a simulation study. Using the best estimates identified in the inverse analysis as the inputs, the moisture diffusion process can be resimulated in the finite element analysis. Then the simulated relative

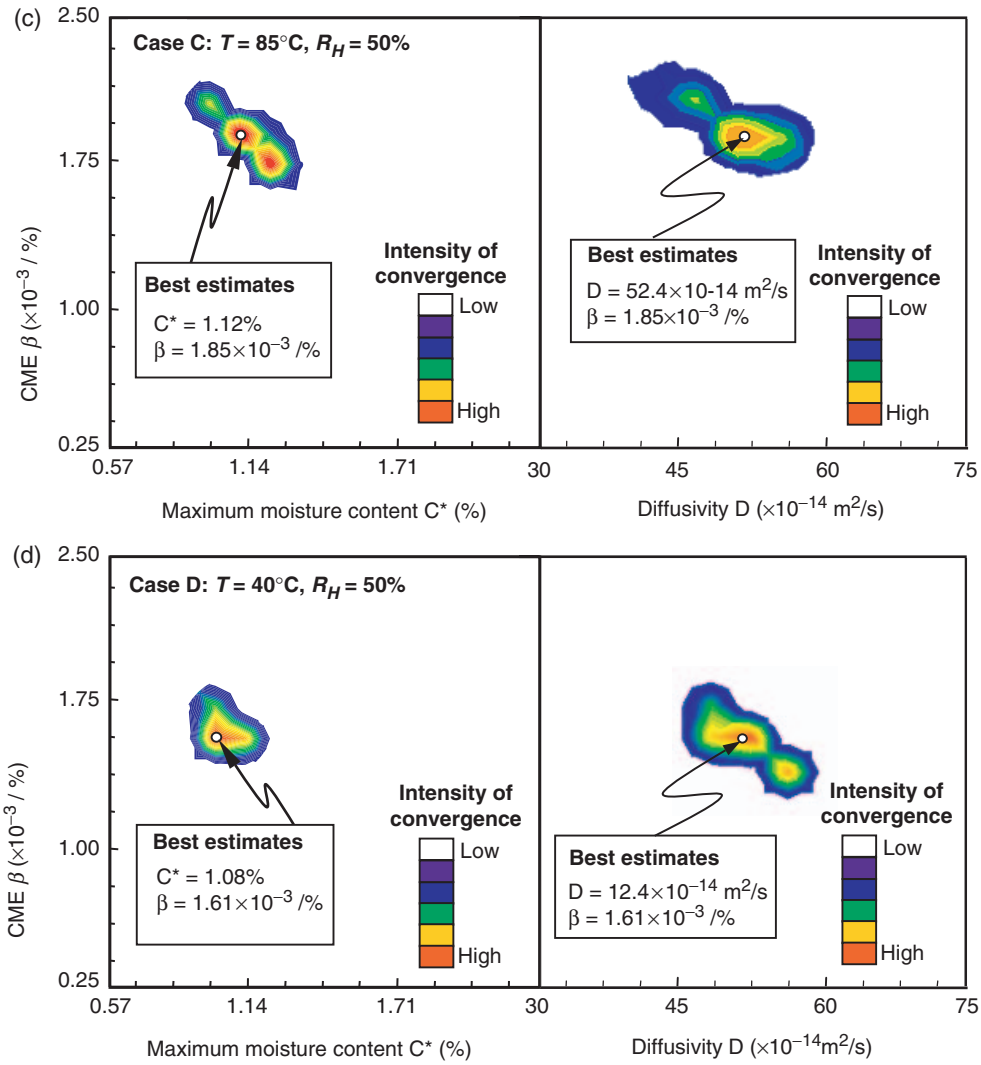

Figure 7. *Continued.*

Table 2. Estimated hygrothermal parameters of epoxy based on inverse analysis for the different environmental conditions.

Exposure conditions				Diffusivity	Max. moist.	
Case	T (°C)	R_H (%)	Time (h)	($\times 10^{-14}$ m^2/s)	content (%)	CME ($\times 10^{-3}$/%)
A	85	85	600	54.3	1.45	1.89
B	40	85	1200	13.2	1.41	1.63
C	85	50	600	52.4	1.12	1.85
D	40	50	1200	12.4	1.08	1.61

Table 3. Estimated hygrothermal parameters of the epoxy based on inverse analysis using shorter periods of experimental measurements (60% of total measured time).

Exposure conditions				Diffusivity	Max. moist.	
Case	T (°C)	R_H (%)	Time (h)	($\times 10^{-14}$ m^2/s)	content (%)	CME ($\times 10^{-3}$/%)
A	85	85	360	55.8	1.49	1.92
B	40	85	720	14.1	1.44	1.69
C	85	50	360	53.5	1.18	1.89
D	40	50	720	13.1	1.13	1.64

weight gains and strain changes are compared with the actual measurements as shown in Figure 8. The agreements between the measured and simulated values are remarkable. Except near the initial phase, the simulated results are well within the bounds of measured oscillations throughout the measured time period. Although the good agreement does not prove the uniqueness, it further supports the accuracy of parameters obtained in the present inverse analysis.

Thermal Expansion

As previously described, the CTE were estimated from separate tests since thermal equilibrium is achieved much faster than moisture saturation. As in the case of moisture expansion, the normal strain perpendicular to the fiber direction was measured in thermal expansion tests. Since strain measurements were made at discrete temperatures, the CTE of composites was determined from the difference in strains at two different temperatures, whose average is reported as the corresponding temperature. As shown in Figure 3, the strains did not exhibit a smooth variation with increasing temperature. Consequently, the computed effective CTE of composite is highly oscillatory during the course of the first heating cycle as shown in Figure 9. As the specimen was reheated, changes in CTE behavior became smoother.

This behavior is investigated here. First, to quantify the scattering at each heating cycle, an index that represents average deviation from linear fit is introduced as

$$s = \frac{1}{N}\sum_{i=1}^{N}\left|\frac{\alpha_i^{\text{meas}} - \alpha_i^{\text{fit}}}{\alpha_i^{\text{fit}}}\right|. \tag{6}$$

Here α_i^{meas} is the ith temperature increment of measured CTE, N is the total measurements, and α_i^{fit} is the CTE of linearly fitted curve (generated from all data) at the ith increment. Note that the standard deviation was not used here since CTE is clearly dependent on temperature. The linear fit and corresponding scattering index for each specimen at selected heating cycles is also shown in Figure 9. As the specimens were repeatedly subjected to thermal cycling, the scattering index was reduced drastically. It was also observed that the linear fit equations were nearly identical for all the heating cycles.

Since repeated heating caused the scattering to subside, it was postulated that stress relaxation occurs during the thermal cycles. Initially, the composites contain locally high residual stresses generated during the manufacturing process. Due to the heterogeneous

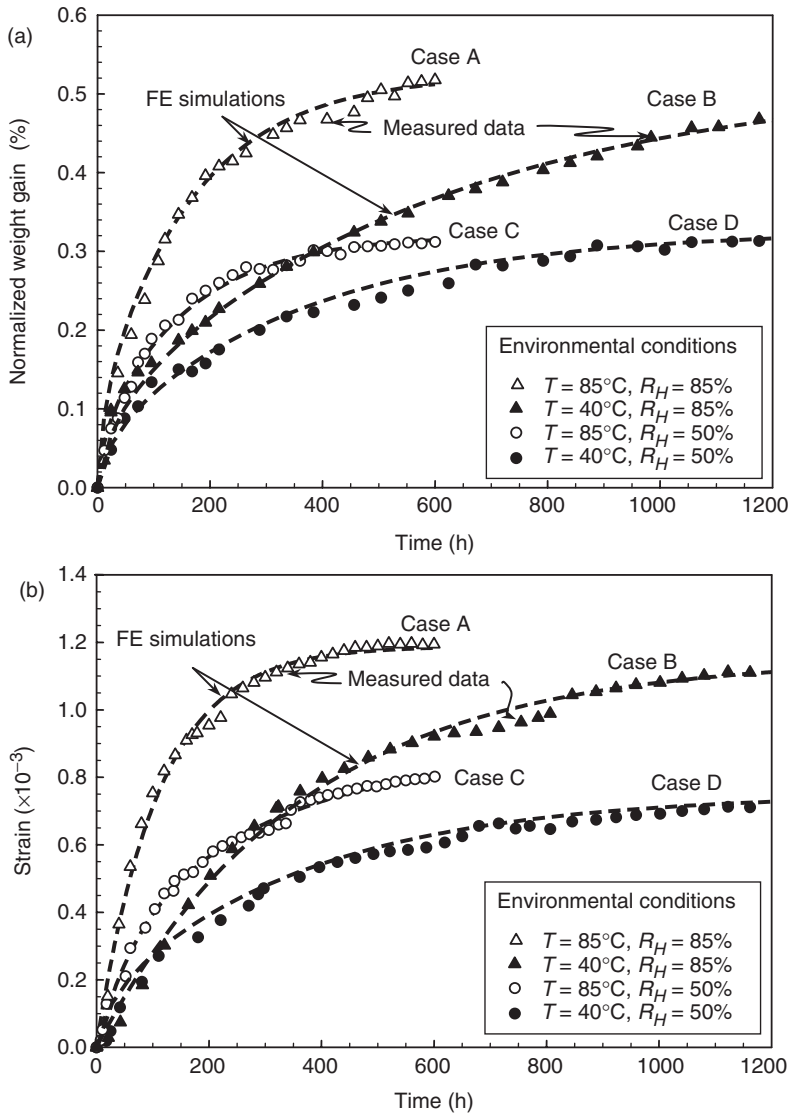

Figure 8. *Comparisons between measured (symbols) and computed (dash lines): (a) weight gain and (b) transverse strain. The latter solutions are obtained from finite element simulations with the best estimates obtained in the inverse analysis.*

nature of microstructure, thermal mismatch is likely to cause stress concentrations near the fiber–epoxy interfaces. When the specimens are heated, these stresses can cause different deformation state through some local microstructural changes such as interface sliding. Although the precise nature of the mechanism governing the reduction in scatter in the thermally induced strains cannot be identified within the scope of the present study, a likely phenomenon is the redistribution of residual stress and deformation fields during cyclic heating. Note that the specimens were heated up to 120°C, which is well below the glass transition temperature of epoxy. Nevertheless, this temperature may sufficiently

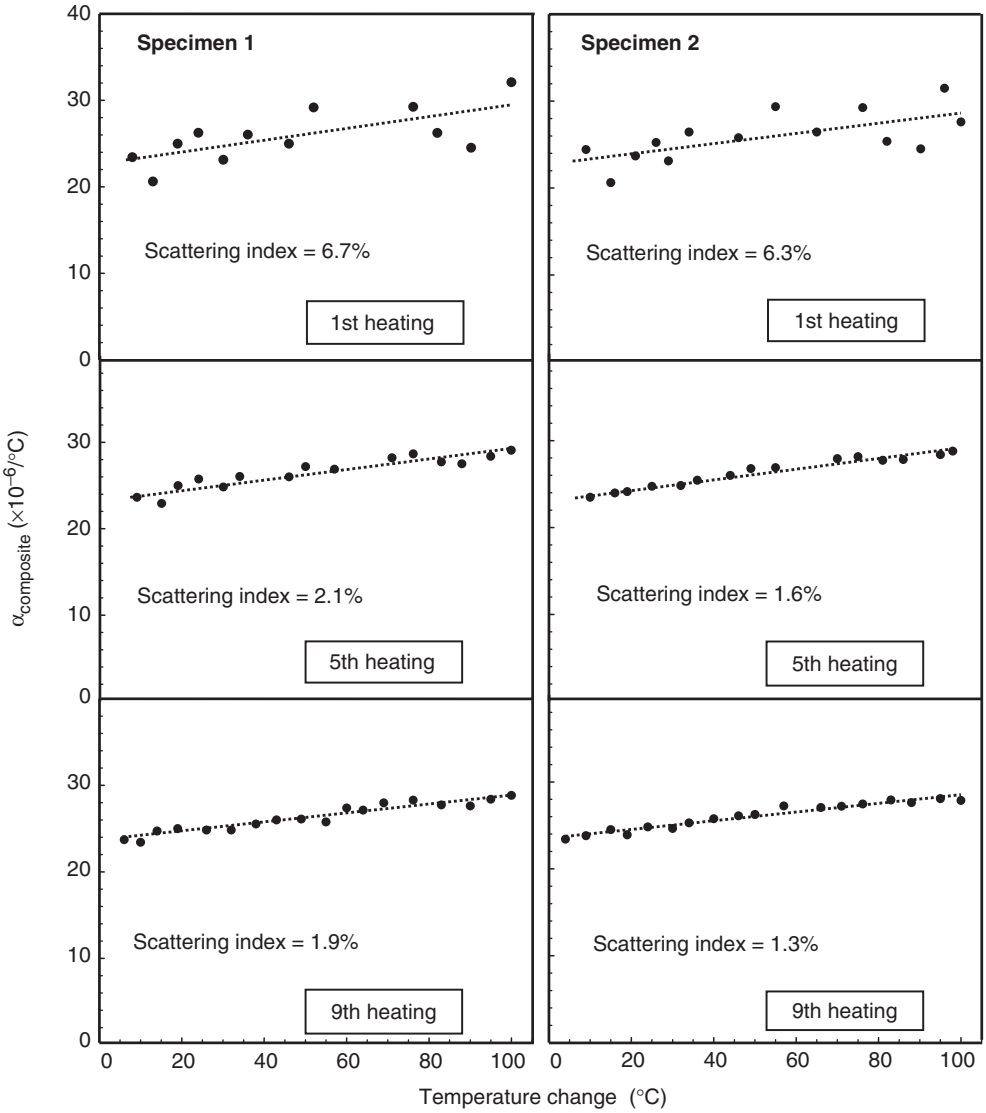

Figure 9. *Variations of CTE with temperature change shown at selected thermal cycles for two different specimens. The dashed line in all plots corresponds to the best linear fit obtained from the 9th heating results.*

soften epoxy to promote the redistributions. After repeated cycles, stresses are more evenly distributed and smoother strain changes prevail.

The uneven behavior of strain observed during moisture absorption, as shown in Figure 2(b), can also be attributed to similar mechanisms. Since these phenomena are local, it is probably difficult to detect them from overall deformation measurements (i.e., via displacement).

Once CTE of composites was determined, the CTE of epoxy was computed based on the linear relationship obtained from the finite element calculations. Here two simulations

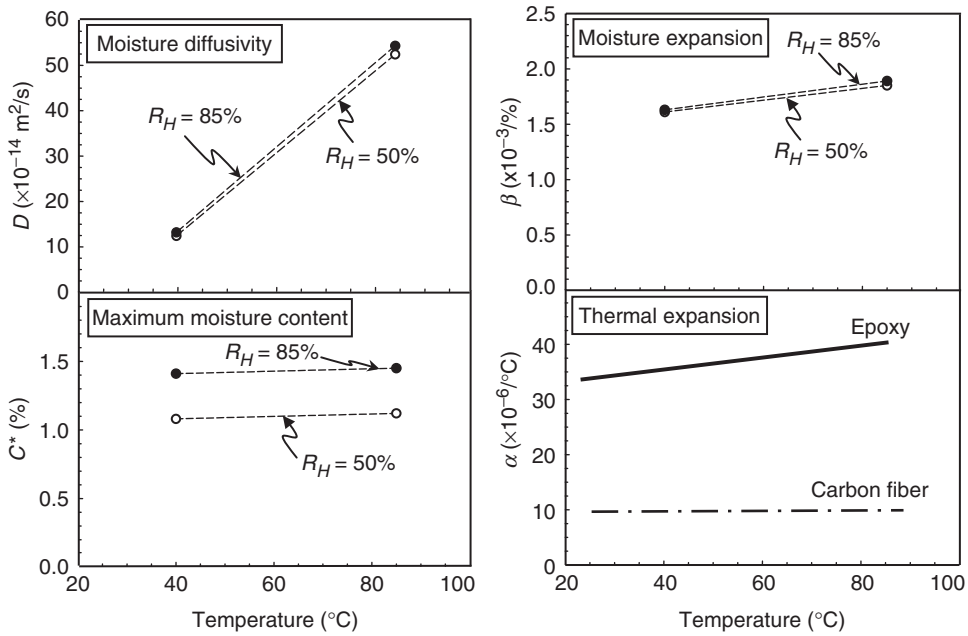

Figure 10. *Temperature and humidity dependence of hygrothermal parameters of epoxy. Note α (CTE) is assumed to be independent of humidity and that of carbon fiber is also shown for reference.*

were performed with different CTE of epoxy, and the effective property of composite was found as $\alpha_{\text{composite}} = 0.60\alpha_{\text{epoxy}} + 0.40\alpha_{\text{carbon}}$. This relation is very close to that obtained using a rule-of-mixtures approach. Using this relation and the linear fit of results during 9th heating, the temperature dependent CTE of epoxy was determined as $\alpha_{\text{epoxy}} = (0.05 \times 10^{-6}/^{\circ}\text{C})\Delta T + \alpha^*_{\text{epoxy}}$, where $\alpha^*_{\text{epoxy}} = 23.5 \times 10^{-6}{}^{\circ}\text{C}$ is the room temperature CTE. During heating from $T = 20$ to 120°C, the CTE increases by about 20%.

Summary of Hygrothermal Properties

In order to illustrate the humidity and temperature dependences of the hygrothermal properties, the estimated parameters of epoxy under different conditions are summarized in Figure 10. Here, the parameters are plotted as functions of temperature for two different humidity conditions except for CTE. It can be observed that diffusivity is a strong function of temperature and a very weak function of relative humidity. In contrast, the maximum moisture content is a strong function of relative humidity and a weak function of the temperature. The CME appears to have a slight dependence on the temperature, but essentially no dependence on humidity. Finally, the CTE exhibited a noticeable increase with temperature. Similar plots can be generated for the effective properties of composites. Essentially they would show similar trends as those for epoxy but with different magnitudes. To obtain corresponding values for the entire composites, the following relations can be used: $C^*_{\text{composite}} = 0.35C^*_{\text{epoxy}}$, $D_{\text{composite}} = 0.224D_{\text{epoxy}}$, $\beta_{\text{composite}} = 0.35\beta_{\text{epoxy}}$, and $\alpha_{\text{composite}} = 0.60\alpha_{\text{epoxy}} + 0.40\alpha_{\text{carbon}}$.

DISCUSSION

In the current analysis, the hygrothermal properties of carbon-fiber reinforced epoxy composites were determined using a novel experiment and inverse analysis-based approach. The specimens were subjected to different environmental conditions, and four critical parameters, namely, diffusivity, maximum moisture content, coefficient of thermal expansion and coefficient of moisture expansion, were estimated. Moisture absorption experiments were performed in a controlled environmental chamber where weight gains and strains were measured. The fiber-optic sensors used to measured strains are well suited for long-term moisture and temperature tests. In this investigation instead of determining the effective properties of composites, those of the matrix epoxy phase were determined since this approach offers certain advantages. Note that a similar procedure can be still used to determine the overall composite properties if desired.

Using the parameters obtained under four different temperature and moisture conditions, the parameters under any other conditions may be estimated through interpolation. Furthermore accumulated expansions and moisture content under varied history of environmental conditions can be estimated from time integrations of known parameters.

The anisotropic nature of moisture transport was not considered (albeit its effect is expected to be substantially less than that of the modulus ratio) and only moisture flow perpendicular to fibers was included in the present study. The moisture flow along the fiber is not usually important since regardless of orientation, fibers are normal to the free-surface in most long-fiber-reinforced composite laminates.

The inverse analysis technique was utilized to obtain best estimates of the unknown hygrothermal material parameters. This analysis is effective when relations between measurements and unknown parameters are not obvious. With this approach, it is possible to simultaneously obtain several unknown parameters from a single test. In other techniques, that involve the step-by-step determination of unknown parameters, any initial error can propagate to the estimation of subsequent parameters. On the other hand, the inverse analysis searches the best estimates of all parameters at the same time and avoids progression of errors. Secondly, in the process of establishing forward solutions, the heterogeneous microstructure of the composite is taken into account. This was found to be essential for transient moisture transport problems. Here a random fiber finite element model, containing over 1000 fibers, was constructed to generate the reference data/ forward solutions.

The inverse analysis procedure was used to produce intensity of convergence plots, from which the best estimates of the hygrothermal parameters were extracted. The sizes of the converged region as well as excellent correlation between the simulated and the measured results support the accuracy of the present estimates. This approach allows the determination of several parameters from a single test. Additionally, this technique can considerably shorten the required exposure period. This feature is especially valuable for experiments that study the environmental influence at lower temperature tests, which generally require very long exposure durations to achieve saturation.

In the present approach, the total number of unknown state parameters was three in the moisture absorption tests, which had made the procedure significantly more complex than the two unknown cases. The maximum number of unknown state parameters that can be estimated effectively in similar problems is probably limited to four. As the number of unknown parameters increase, not only does the analysis require more

complex reference/forward solutions, but also the convergence behavior tends to deteriorate. This occurs because several combinations of parameters may yield similar results (i.e., measured parameters). One way to accommodate a greater number of unknowns is to estimate the parameters sequentially. The separations of the unknown parameters then must be carried out in accordance with their influence on the measured parameters. However, as noted earlier, such a procedure may have problems of initial error propagation.

ACKNOWLEDGMENTS

This material is based upon work supported by, or in part by, the National Science Foundation under grant number CMS 0219250, US Army Research Laboratory, and the US Army Research Office under contract/grant number DAAD19-02-1-0333. We are also thankful to the authors J. Morris and S. Fattohi of Cytec Engineered Materials, Inc., Anaheim, CA for donating IM7/997 composite laminates.

APPENDIX

Fiber optic sensors use a thin layer of epoxy as an adhesive for surface bonding. This epoxy layer may then act as a barrier to moisture absorption and consequently alter the expansion measurements. Here, such effect is quantified through a detailed computational analysis with two separate models. Note the weight gain was measured with separate specimens but that would not have made any difference since the area covered by the epoxy layer is less than 0.1% of the total surface area of the laminate.

In the first model, a 100 μm thick layer of epoxy was added to the existing 2D model with many discretely modeled fibers shown in Figure 6(b). In this case, the moisture content is provided as the boundary condition at the top of the new epoxy layer while the strain is measured at the middle of the epoxy layer. Since the symmetric conditions were assumed, the layer is modeled to extend entire free surfaces in front and back. The computation was carried out for Case A ($T = 85^{\circ}$C and $R_H = 85\%$), and the transverse strain at the middle of extra layer was recorded (i.e., physical mid-point location of fiber-optic sensor). This strain was normalized with the computed strain reported in Figure 8(b) and noted as 2D model in Figure A1. The results show initial discrepancy but for $t > 180$ h, the two results were essentially identical.

In order to evaluate the effects of geometry, a full 3D model representing the entire specimen was also constructed. Here the moisture transport occurs through all directions and faces. The 3D model ($70 \times 35 \times 1.2$ mm) was constructed with about 180,000 nodes and 800,000 tetrahedral elements. Due to the size of the mesh, it was not possible to discretely model fibers and a homogenized model with effective properties was used. Two computations were performed, with and without the epoxy layer ($7.5 \times 10 \times 0.1$ mm). The strain computed from the model with the epoxy layer was normalized with that from the one without the layer and is shown in Figure A1. As in the case of 2D, one can observe some initial discrepancy that disappears as time progresses. Since the actual area covered by the epoxy is more accurately modeled here, the effect of the layer was less than that of the 2D model. Both models attest the effects of extra epoxy layer used to cover fiber-optic sensor to be minimal. These results, however, suggest that sufficient data beyond $t = 180$ h

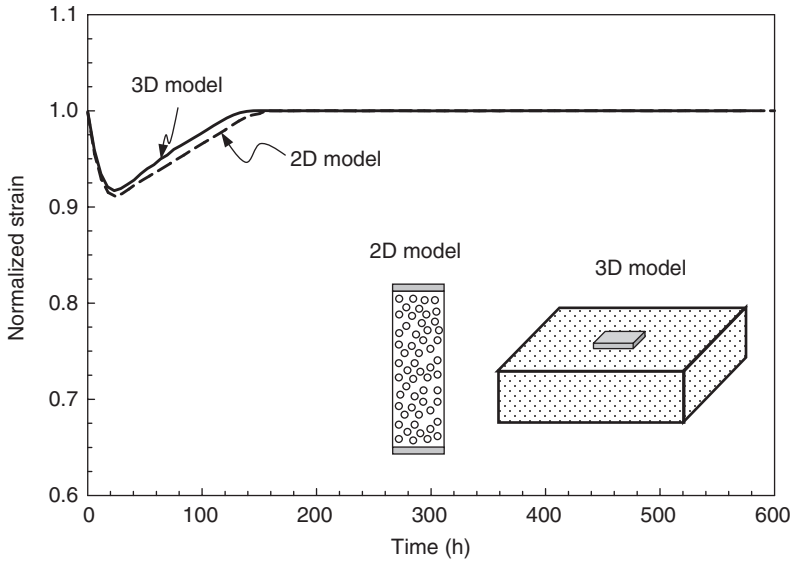

Figure A1. *Strains obtained with extra epoxy layer are normalized with corresponding strains without the layer for the 2D and 3D models. Note that schematics in the figure are not drawn in correct scale.*

must be provided in the inverse analysis. The estimates from shorter time period shown in Table 3 used the first 360 h of data.

REFERENCES

1. Lee, M.C. and Peppas, N.A. (1993). Models of Moisture Transport and Moisture Induced Stresses in Epoxy Composites, *Journal of Composite Material*, **27**(12): 1146–1171.
2. Weitsman, Y.J. (1991). *Fatigue of Composite Materials*, Elsevier, New York.
3. Jones, F.R. (1999). *Reinforced Plastics Durability*, Woodhead Publishing Company, Cambridge.
4. Zheng, Q. and Morgan, R.J. (1993). Synergistic Thermal-moisture Damage Mechanisms of Epoxies and their Carbon-fiber Composites, *Journal of Composite Materials* **27**(15): 1465–1478.
5. Bhavesh, G.K., Singh, R.P. and Nakamura, T. (2002). Degradation of Carbon Fiber Reinforced Epoxy Composites by Ultraviolet Radiation and Condensation, *Journal of Composite Materials*, **36**(24): 2713–2733.
6. Adams, R.D. and Singh, M.M. (1996). The Dynamic Properties of Fiber-reinforced Polymers Exposed to Hot, Wet Conditions, *Composites Science and Technology*, **56**(8): 977–997.
7. Zhao, S.X. and Gaedke, M. (1996). Moisture Effects on Mode II delamination behavior of Carbon/Epoxy Composites, *Advanced Composites Materials*, **5**(4): 291–307.
8. Choi, H.S., Ahn, K.J., Nam, J.D. and Chun, H.J. (2001). Hygroscopic Aspects of Epoxy/Carbon Fiber Composite Laminates in Aircraft Environments, *Composites Part A–Applied Science and Manufacturing*, **32**(5): 709–720.
9. Soutis, C. and Turkmen, D. (1997). Moisture and Temperature Effects of the Compressive Failure of CFRP Unidirectional Laminates, *Journal of Composite Materials*, **31**(8): 832–849.
10. Sala, G. (2000). Composite Degradation Due to Fluid Absorption, *Composites Part B-Engineering*, **31**(5): 357–373.
11. Asp, L.E. (1998). The Effects of Moisture and Temperature on the Interlaminar Delamination Toughness of a Carbon/Epoxy Composite, *Composite Science and Technology*, **58**(6): 967–977.

12. Patel, S.R. and Case, S.W. (2000). Durability of a Graphite/Epoxy Woven Composite Under Combined Hygrothermal Conditions, *International Journal of Fatigue*, **22**(9): 809–820.
13. Loos, A.C. and Springer, G.S. (1979). Moisture Absorption of Graphite-epoxy Composites Immersed in Liquids and in Humid Air, *Journal of Composite Materials*, **13**(1): 131–147.
14. Vaddadi, P., Nakamura, T. and Singh, R.P. (2003). Inverse Analysis for Transient Moisture Diffusion Through Fiber Reinforced Composites, *Acta Materialia*, **51**(1): 177–193.
15. Fitzgerald, S.B., Kalamkarov, A.L. and MacDonald, D.O. (1999). The Use of Fabry Perot Fiber Optic Sensors to Monitor Residual Strains During Pultrusion of FRP Composites, *Composites Part B*, **30**(2): 167–175.
16. Lawrence, C.M., Nelson, D.V., Bennett, T.E. and Spingarn, J.R. (1997). Determination of Process-induced Residual Stresses in Composite Materials Using Embedded Fiber Optic Sensors SPIE, *Proceedings on Smart Structures and Materials*, **3042**: 154–165.
17. Zhao, Y. and Farhad, A. (2002). Embedded Fiber Optic Sensor for Characterization of Interface Strains in FRP Composites, *Sensors and Actuators A*, **100**(2–3): 247–251.
18. Morris, J. (2001). *Private Communication*, Cytec-Fiberite, Inc., California.
19. Kalman, R.E. (1960). A New Approach to Linear Filtering and Prediction Problems, *ASME Journal of Basic Engineering*, **82D**: 35–45.
20. Grewal, M.S. and Andrews, A.P. (1993). *Kalman Filtering: Theory and Practice*, Prentice-Hall, Inc., New Jersey.
21. Yibing, W. and Papageorgiou, M. (2005). Real-time Freeway Traffic State Estimation Based on Extended Kalman Filter: A General Approach, *Transportation Research Part B: Methodological*, **39**(2): 141–167.
22. Michael, P. and Phillip, A.L. (2003). Kalman Filter Recipes for Real-time Image Processing, *Real-Time Imaging*, **9**(6): 433–439.
23. Hoshiya, M. and Saito, E. (1984). Structural Identification by Extended Kalman Filter, *Journal of Engineering Mechanics*, **110**(12): 1757–1770.
24. Aoki, S., Amaya, K., Sahashi, M. and Nakamura, T. (1997). Identification of Gurson's Material Constants by Using Kalman Filter, *Computational Mechanics*, **19**(6): 501–506.
25. Nakamura, T., Sampath, S. and Wang, T. (2000). Determination of Properties of Graded Materials by Inverse Analysis and Instrumented Indentation, *Acta Materialia*, **48**(17): 4293–4306.
26. ABAQUS v6.5, 2004, HKS inc., Pawtucket, RI.
27. Lundgren, J.E. and Gudmundson, P. (1999). Moisture Absorption in Glass Fiber/Epoxy Laminates with Transverse Matrix Cracks, *Composite Science and Technology*, **59**(13): 1983–1991.